ACS OMEGA

http://pubs.acs.org/journal/acsodf

Article

Deep-Sintered Copper Tracks for Thermal Oxidation Resistance Using Large Pulsed Electron Beam

Yunjae Hwang, Jisoo Kim,* Changyong Yim,* and Hyung Wook Park*

Cite This: *ACS Omega* 2021, 6, 19134−19143

Read Online

ACCESS | Metrics & More | Article Recommendations | Supporting Information

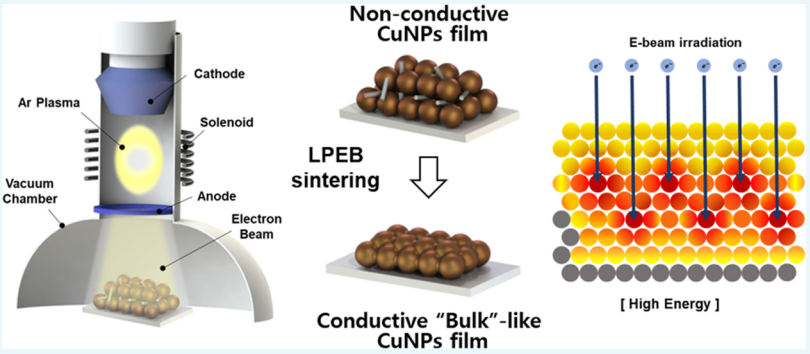

ABSTRACT: Thermal oxidation resistance is an important property in printed electronics for sustaining electrical conductivity for long time and/or under harsh environments such as high temperature. This study reports the fabrication of copper nanoparticles (CuNPs)-based conductive tracks using large pulsed electron beam (LPEB) by irradiation on CuNPs to be sintered. With an acceleration voltage of 11 kV, the LPEB irradiation induced deep-sintering of CuNPs so that the sintered CuNPs exhibited bulk-like electrical conductivity. Consequently, the sintered Cu tracks maintained high electrical conductivity at 220 °C without using any thermal oxidation protection additive, such as silver, carbon nanotube, and graphene. In contrast, the films irradiated with an acceleration voltage of 8 kV and irradiated by intense pulsed light (IPL) showed fast oxidation characteristics and a corresponding reduction of electrical conductivities under high temperatures owing to a thin sintered layer. The performance of highly thermal oxidation-resistant Cu films sintered by LPEB irradiations was demonstrated through the device performance of a Joule heater.

1. INTRODUCTION

The interest in printed electronics is continuously increasing because of the requirement of form factors in the production of electronic devices comprising complex shapes and large scales, following the miniaturization of the electronic devices and mass production.[1,2] The key advantages of printed electronics compared with traditional methods, such as photolithography, vacuum deposition, electro- and/or electroless-plating processes, are low-cost manufacturing, high throughput, eco-friendliness, waste minimization, and the possibility of patterning.[3,4] Additive inkjet printing, which enables high-resolution pattering, and roll-to-roll (R2R) technique, which enables high throughput patterning, are attractive technologies for direct printed electronics. These electronics printing technologies can be adopted in various industrial fields such as radio frequency identification tags, printed circuit boards, thin-film transistors, light-emitting devices, and heaters.[1,4−6]

One of the most important aspects in the manufacturing of printed electronics is the selection of materials that can determine the electrical properties, especially conductivity. Conducting polymers, graphene, carbon nanotube (CNT), silver nanowire, copper nanofiber, and metallic nanoparticle (NP) inks are representative materials for printed electronics as electrode materials.[7−16] Among them, the inks using metallic NPs such as silver (Ag), gold (Au), and copper (Cu) NPs are gaining considerable interest for their use in printed electronics owing to their superior electrical conductivity, cost-effectiveness, and easy manufacturing processes.[15−18] Generally, noble metals, such as Ag and Au, are widely used because of their superior electrical properties and high oxidation resistance.[16−18] Recently, Ag and Au have been replaced by Cu as it exhibits similar electrical conductivity and is more economical than other noble metals.[19,20] However, pure metallic NP films are nonconductive because of the high contact resistance between each NP; therefore, they require post-treatment to be conductive.[17,21] Various post-treatment methods have been introduced, such as thermal annealing,[17]

Received: May 11, 2021
Accepted: July 1, 2021
Published: July 13, 2021

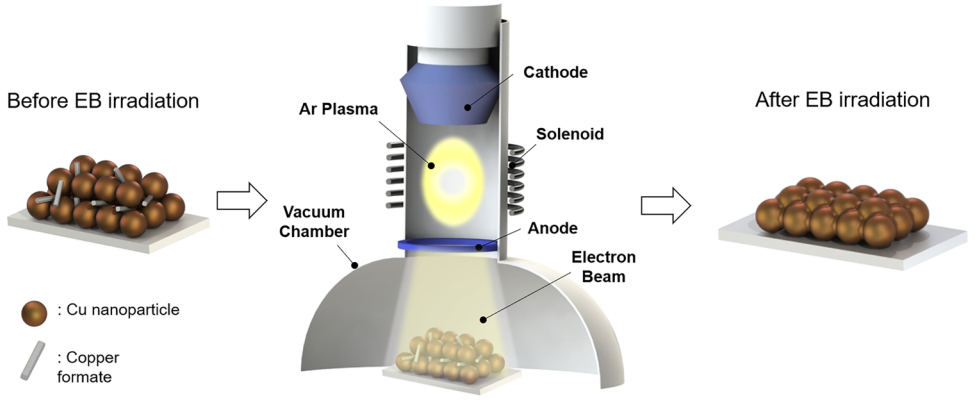

Figure 1. Schematic diagram of the sintering process of copper nanoparticles using large pulsed electron beam (LPEB) irradiation.

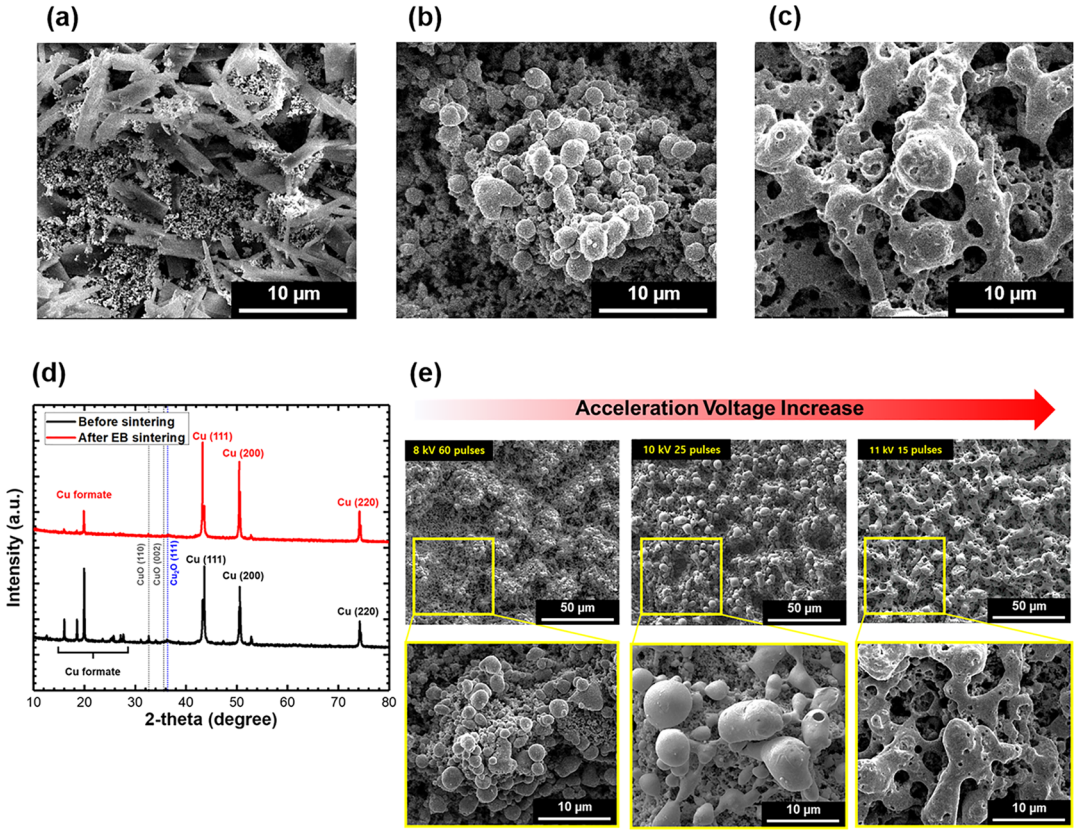

Figure 2. Scanning electron micrographs of (a) the as-prepared copper film and after LPEB sintering process under the (b) low energy (LE) and (c) high energy (HE) conditions. (d) X-ray diffraction patterns of copper films before and after LPEB irradiation. (e) Variation in the morphology of the copper films by increasing the irradiation energy of LPEB.

selective laser sintering,[22−24] and intense pulsed light (IPL) irradiations.[25] However, these post-treatments have some limitations, for instance, the thermal annealing process cannot be adopted for patterning of conductive tracks. Moreover, the processing parameters of selective laser sintering should be carefully selected because the absorptivity of the laser changes as a function of wavelength. Most recently, the IPL sintering method has attracted considerable attention owing to the exposure of high energy (HE) to a large area within several milliseconds. However, the sintered Cu electrode irradiated by IPL has a relatively less thickness; therefore, it can be easily oxidized.[19,20,26,27] Moreover, Cu itself has relatively high thermal oxidation tendency compared with other noble metals.[28,29] Although naturally formed oxides have sub-nanoscale thickness, they critically degrade the original electrical and mechanical properties because the size of particles is only several nanometers. This characteristic restricts applications such as Joule heating in a high-temperature environment that accelerates oxidation.[19,20,29] To overcome the limitation of CuNP-based electrodes, several studies have adopted hybrid inks such as copper−silver, copper−silver−CNT, and copper−silver−graphene.[19,20,30,31] However, research on post-treatment processes aiming to improve the oxidation resistance is yet to be explored using only CuNPs.

This study introduces a novel sintering technique for metallic NPs using large pulsed electron beam (LPEB) irradiation. The LPEB has been adopted not only for modifying the surfaces of a variety of metals and alloys but

https://doi.org/10.1021/acsomega.1c02475
ACS Omega 2021, 6, 19134−19143

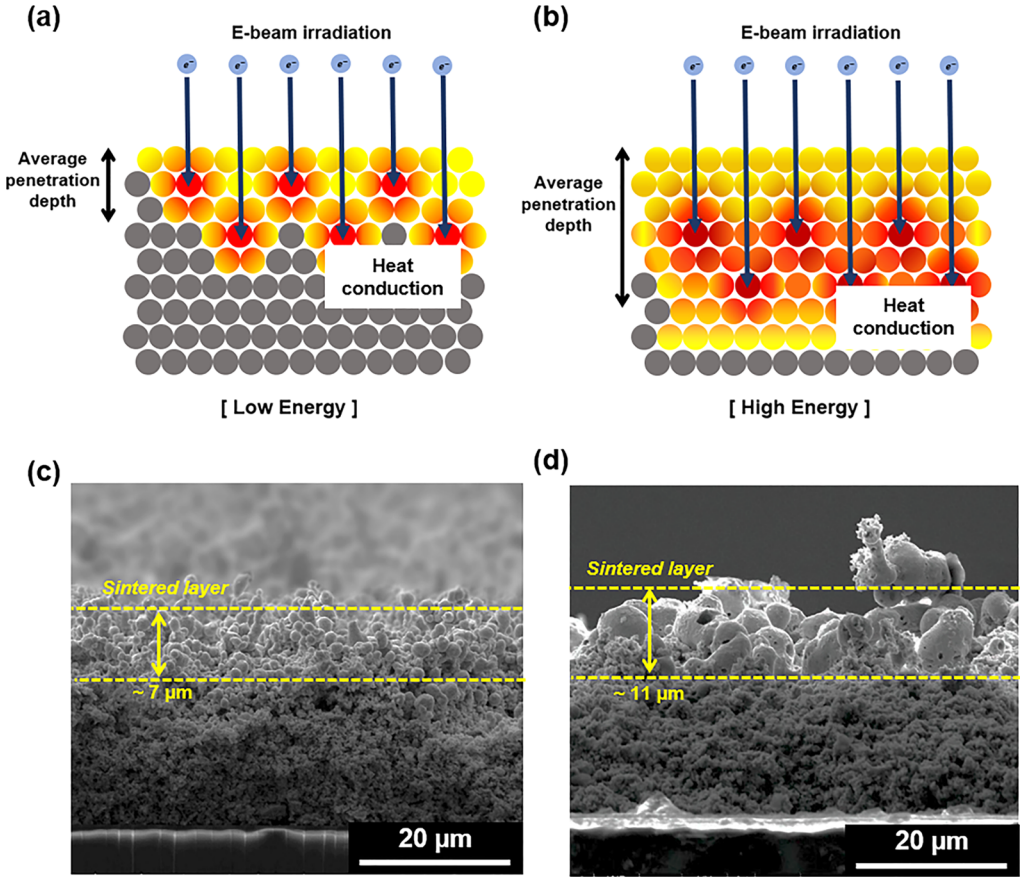

Figure 3. Schematic diagram of the energy transfer from a large pulsed electron beam to copper films under the (a) LE and (b) HE conditions. Corresponding cross-sectional scanning electron micrographs of copper films sintered under the (c) LE and (d) HE conditions.

also for improving mechanical and chemical properties,[32,33] welding silver nanowires,[34] and additive manufacturing.[35,36] However, a few studies investigating the sintering process of metallic NP inks using electron beam irradiation have been reported. In our approach, a formic-acid-treated CuNP ink (F-Cu ink) was sintered using the LPEB irradiation to enhance the thermal oxidation resistance of the CuNP-based electrodes. The printed Cu film, which was initially nonconductive, turned into a conductive electrode using the LPEB sintering process. Various sets of acceleration voltage and number of pulses were tested to optimize the sintering condition. The performance of LPEB-sintered Cu tracks under high-temperature conditions was quantitatively evaluated by measuring the electrical conductivity with respect to time. Morphological variations and different oxidation tendencies depending on the LPEB parameters were specified using microstructural analysis. Finally, the performance of LPEB-sintered Cu tracks was demonstrated through a Joule heater.

2. RESULTS AND DISCUSSION

2.1. Nanostructures of LPEB-Sintered Cu Tracks.

Figure 1 presents the scheme of LPEB sintering process. Scanning electron microscopy (SEM) image of the Cu film before LPEB irradiation is shown in Figure 2a. The unsintered Cu film exhibited a rod-shaped structure and the presence of CuNPs. The rod-shaped structures are formed by chemical reactions of Cu and HCOOH.[19,37] Before LPEB irradiation, HCOOH treatment is performed to convert the Cu oxide to Cu formate according to the following reactions[19]

$$Cu + 2HCOOH \rightarrow Cu(HCOO)_2 + H_2 \quad (1)$$

$$CuO + 2HCOOH \rightarrow Cu(HCOO)_2 + H_2O \quad (2)$$

After LPEB irradiation, the Cu formate and CuNPs absorbed the heat energy generated by accelerated electrons, which have a high kinetic energy.[34] The energy transferred from LPEB was enough to decompose the Cu formate and melt the CuNPs (represented by eq 3), thereby eliminating the rod-shaped structures and aggregating the CuNPs, as shown in Figure 2b,c.

$$Cu(HCOO)_2 \rightarrow Cu + 2CO_2 + H_2 \quad (3)$$

The transformation of Cu formate into conductive Cu was verified by X-ray diffraction (XRD) in Figure 2d to specify the effect of LPEB on the Cu films. In Figure 2d, the unsintered Cu film exhibits three peaks at 43.6, 51, and 74.2° that represent (111), (200), and (220) crystal planes of Cu, respectively. The weak peaks at 32.5, 35.5, and 36.6° corresponded to CuO(110), CuO (002), and Cu_2O(111) crystal plane. Additionally, the unsintered Cu film shows several peaks in the range of $14 \leq 2\theta \leq 38°$, which indicate the presence of Cu formate because most of these peaks are removed after LPEB irradiation. Also, the weak peaks related to Cu oxide are removed after LPEB irradiation, indicating the reduction of CuO and Cu_2O to Cu. Moreover, the peak intensities of Cu(111), (200), and (220) slightly increases, indicating that the transformation of Cu formate into Cu was conducted by the aforementioned chemical reaction (eq 3).[20] This transformation of Cu formate to Cu can also be seen in the X-ray photoelectron spectroscopy (XPS) image in Figure

https://doi.org/10.1021/acsomega.1c02475
ACS Omega 2021, 6, 19134−19143

S1. Figure S1a shows the high-resolution C1s spectrum of unsintered Cu film with four peaks. Among the four peaks, the peak at 288.3 eV is attributed to the O=C−O bond, which is related to the formate molecule.[38] After the LPEB irradiation, the peak at 288.3 eV decreases following the increasing energy of LPEB, as shown in Figure S1b,c, indicating the decomposition of the Cu formate.

Figure 2e shows the changes in the morphology of the aggregated Cu particles after LPEB sintering, based on the intensity of irradiated energy (acceleration voltage). Shallowly melted Cu liquid formed under the LE condition clumped into the micron-scale (∼2 μm) spherical Cu particles when resolidified (Figure 2b). By increasing the energy intensity, larger spherical Cu particles were formed. Finally, deeply melted Cu particles irradiated by sufficient energy (HE) started to form well-linked Cu webs (Figure 2c). This morphological change is in agreement with Ostwald ripening.[39−41] Ostwald ripening introduces the growth mechanism of nanoparticles during sintering with a liquid phase. Thermodynamically, to reduce the energy instability from the difference in the surface-to-volume ratio between large and small particles, adatoms on the surface of small particles with a high surface energy diffuse to the surface of large particles, which are relatively stable in terms of surface energy. Large particles grow at the expense of smaller particles and form spherical shapes due to surface tension. Finally, as the size increases, the gravity force becomes more dominant than the surface tension, failing to maintain its spherical shape and subsequently forming the web shape.

2.2. Sintering Mechanism Using LPEB. Although several factors affect the total energy transfer of LPEB irradiation, the energy of LPEB sintering can be mainly controlled by the acceleration voltage and the number of pulses. Especially, the acceleration voltage is closely related to the sintered layer thickness owing to the transmission of accelerated electrons. The effect of acceleration voltage on the sintered layer thickness can be estimated simply by the penetration depth determination. Within the maximum penetration depth, electrons transmit their kinetic energy to the substrate with a small energy loss. Previously, the relation between the penetration depth of accelerated electrons and the acceleration voltage was well defined as follows[42]

$$\delta = \frac{2.76 \times 10^{-2}\ \mathrm{mol/m^2} \times m_A \times N_A \times (E_0/\mathrm{keV})^{5/3}}{Z^{8/9}} \times \frac{(1 + 0.978 \times 10^{-3} \times E_0/\mathrm{keV})^{5/3}}{(1 + 1.957 \times 10^{-3} \times E_0/\mathrm{keV})^{5/3}} \times \frac{1}{\rho} \quad (4)$$

where δ is the penetration depth of the accelerated electrons; E_0 is the incident energy, which is proportional to the acceleration voltage; m_A is the atomic mass of the solid target; N_A is Avogadro's number; Z is the atomic number; and ρ is the density. According to eq 4, the maximum penetration depth is proportional to the acceleration voltage. Furthermore, the electron beam absorptivity in terms of depth is also well established and experimentally validated.[33] Figure 3a,b shows the schematic diagrams of the heat transfer process of LPEB irradiation, based on the energy intensity (acceleration voltage). Because of their porous structure, the accelerated electrons nonuniformly penetrate the Cu film. As stated in the previous study, the heat conduction starts from the depth absorbing the maximum energy.[42] In the case of LE condition, the accelerated electrons have a lower average penetration depth than that of the HE condition. Moreover, the heat conduction effects are narrower because of the lower energy of accelerated electrons compared to that of HE. These different interactions of electrons depending on the intensity were satisfactorily projected in cross-sectional SEM images. As shown in Figure 3c, the thickness of the Cu film decreased from 50 to ∼29 μm and the ∼7 μm thick sintered layer of Cu film was formed under the LE condition. For the HE condition, the thickness of the Cu film decreased to 25 μm and the ∼11 μm thick sintered layer of Cu film was formed as shown in Figure 3d. The thicker sintered layer under the HE condition compared with that from the LE condition can be attributed to the penetration of electrons. Different from the LPEB irradiation, the IPL emitted from a xenon lamp can sinter only the surface of the Cu films due to its long wavelength (580 nm), which was mostly absorbed at the surface of Cu films.[19] As shown in Figure S2a, the thickness of the Cu film decreased to ∼33 μm and a relatively thin thickness of sintered layer on the IPL-sintered sample (∼2 μm) was observed compared to LPEB-irradiated Cu films. Furthermore, the sintered layers irradiated by LPEB showed a different morphological structure of the cross-sectional Cu film by Ostwald ripening. Under the LE condition, a sintered Cu film exhibited a cactus-like structure due to the shallow melting of CuNPs and narrow heat conduction effect (shown in Figure S3a), resulting in the poor connectivity between each CuNPs. Owing to many pores caused by the cactus-like structure, the Cu film under the LE condition showed a low conductivity (∼3.0 Ω). In contrast, the HE condition facilitated the sintering of CuNPs into a bulk-like structure due to the deep melting and wide heat conduction effect (Figure S3b) of particles. Consequently, a higher electrical conductivity (∼1.2 Ω) was obtained due to the well- and deep-sintered layer.

2.3. Surface Oxidation and Electrical Conductivity of Cu Tracks. The change of electrical conductivity of CuNPs-based printed tracks due to thermal oxidation is a well-known phenomenon.[19,20] The mechanism of surface oxidation on Cu substrates can be briefly summarized in two steps: (1) Cu on the gas−solid interface reacts with oxygen rapidly, producing the CuO nanoislands, and (2) the CuO nanoislands grow and form a thin CuO layer.[43] In the case of bulk metals, the electrical conductivity can be maintained despite the formation of a natural oxide layer on the top surface because electrons change their conductive path tunneling through the surface oxide layer. This can be facilitated by the extremely low thickness of natural oxides.[44] The transmission coefficient of electrons, TM_{coeff}, can be simply estimated as follows[45]

$$TM_{coeff} \approx \exp\left(\frac{-4\pi\sqrt{2m(V_0-E)}}{h}L\right) \quad (5)$$

where m is the mass of electrons; h is Planck's constant; V_0 is the barrier potential, which is an inherent property of materials; E is the kinetic energy of electrons; and L is the thickness of oxides. As shown in eq 5, the tunneling transmission coefficient dramatically decreased with increasing thickness of the oxide layers when the applied voltage is constant, indicating constant E. Therefore, it is important to maintain the low thickness of natural oxide layer for better electrical conductivity of metallic tracks. However, the oxidation process of metallic NPs is clearly different from bulk metals. The electrical conductivity of NP-based

https://doi.org/10.1021/acsomega.1c02475
ACS Omega 2021, 6, 19134−19143

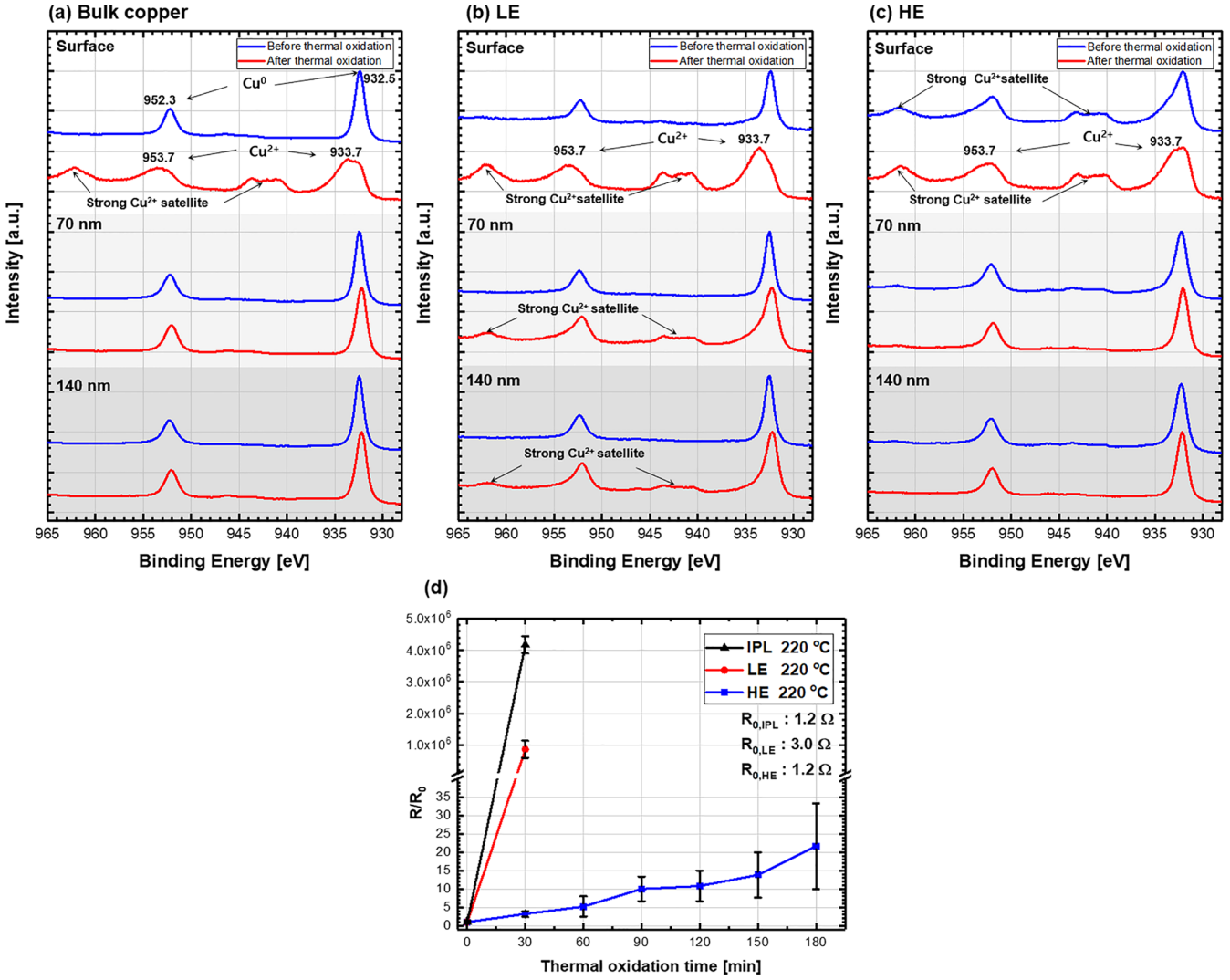

Figure 4. X-ray photoelectron spectra before and after surface etching on (a) bulk copper and LPEB-sintered copper films under the (b) LE and (c) HE conditions. (d) Variation of resistance following the thermal oxidation process.

conductive tracks can be easily degraded by oxidation because separately existing NPs attain a larger surface area contacting the air.[29,46] Thus, all CuNPs on the track are individually oxidized when exposed to the air. It implies that the changes in the electrical conductivity on LPEB-sintered Cu films under the LE and HE conditions can be different, following the thermal oxidation. Because the CuNPs sintered under the HE condition obtained more bulk-like microstructures compared with those obtained from the LE condition (Figure 3d), the subsurface of sintered layer under the HE condition can be effectively protected from the formation of CuO nanoislands. This was verified by XPS analysis of Cu films before and after the thermal oxidation processes. As the oxidation depth is the most important parameter determining the electrical conductivity of films, a depth profiling technique of XPS analysis was adopted. Thermal oxidation tests proceeded at 220 °C for 3 h.

As shown in Figure 4a, the bulk Cu before the thermal oxidation test (as-polished bulk Cu) exhibits intense peaks of Cu^0 (932.5 and 952.3 eV). After thermal oxidation, on the surface, the intense peaks of Cu^{2+} (933.7 and 953.7 eV) become dominant, whereas the peak intensities of Cu^0 decreased. Additionally, the Cu^{2+} satellites, which provide evidence for the formation of CuO, are observed at approximately 943 and 962 eV after thermal oxidation. These XPS results indicate that the top surface of bulk Cu was entirely covered with CuO nanoislands.[43] At 70 and 140 nm depths from the surface, no oxide-related peaks were observed in the spectra even on the thermally oxidized bulk Cu, indicating the absence of oxidation. Consequently, it can be concluded that the bulk Cu exhibited a thin copper oxide layer at the top surface, which was not enough to hinder the electrical conduction, as shown in Figure S4.

In Figure 4b, the Cu film sintered by LPEB irradiation under the LE condition shows dominant and intense peaks of Cu^0 same as the bulk Cu before thermal oxidation regardless of the depth (detail peak deconvolution in Figure S5a,b). After thermal oxidation of the film sintered by the LE condition, Cu^{2+} peaks and Cu^{2+} satellites were generated not only on the surface but also inside of the Cu film, as shown in Figure S5c,d, indicating the presence of independently formed CuO nanoislands inside the film. Owing to the aforementioned microstructures, shallowly sintered CuNPs, and poor connectivity, Cu tracks irradiated under the LE condition are vulnerable to deep oxidation, inducing the formation of a CuO layer on the outermost surface of each NP. Therefore,

https://doi.org/10.1021/acsomega.1c02475
ACS Omega 2021, 6, 19134−19143

Table 1. Comparison of Different Post-Treatment Techniques[a] [51,52]

	substrate after post-treatment	patternability	large-scale sintering possibility	pressure condition	processing time	thickness of sintered layer	oxidation resistance
thermal annealing[51]	poor	poor	good	vacuum	∼1 h		poor
intense pulsed light (IPL)	good	moderate	good	ambient	<20 ms	∼2 μm	poor
laser sintering[52]	good	good	poor	ambient	0.625 mm^2/s	∼1 μm	poor
large pulsed electron beam (LPEB)	moderate	moderate	good	vacuum	∼20 min	∼11 μm	good

[a]Thermal annealing, intense pulsed light (IPL), laser sintering, and large pulsed electron beam (LPEB) are compared in terms of pressure condition, processing time, substrate damage, large-scale sintering possibility, patternable, the thickness of sintered layer, and oxidation resistance.

following further oxidation under high temperatures can be proceeded over the entire thickness.

Figure 4c shows the XPS spectra of the Cu film sintered by LPEB irradiation under the HE condition. Interestingly, in Figure S6a, the peaks of Cu^{2+} and Cu^{2+} satellites are observed on the top surface before thermal oxidation. And these peaks weaken at 70 nm from the surface, as shown in Figure S6b, indicating the formation of a thin CuO layer before thermal oxidation. After thermal oxidation, at the surface, the peaks of Cu^{2+} and Cu^{2+} satellites only slightly increase in Figure S6c due to the small area exposed to air. At the 70 nm depth in Figure S6d, peak locations are preserved without any effect of thermal oxidation compared to that before thermal oxidation. The preformed oxide layer on the surface before thermal oxidation can be attributed to the reaction between the oxygen ion and Cu film. During LPEB irradiation, the remaining oxygen in the chamber can be ionized, which then reacts with the liquid-state Cu under repeated melting and resolidification processes. Consequently, the stable and passive oxide layer, which is different from CuO nanoislands, can be formed through LPEB irradiation. It is well known that the LPEB facilitates the formation of a metallic oxide layer during the LPEB irradiation process, and this suppresses further oxidation.[47−50] Furthermore, the morphological characteristics of LPEB-sintered CuNPs under the HE condition, including well- and thick-sintered layer and small surface area, can effectively prevent the formation of CuO nanoislands on each CuNP. As the top surface of the Cu film was well sintered through LPEB irradiation under the HE conditions, the NPs underneath the sintered layer were not significantly exposed to the air, thereby preventing the oxidation reaction.

These results are also well supported by the quantitative approaches. At the surface, the areal fraction related to the Cu^{2+} peaks of the Cu film under the LE condition significantly increased to 80.45% after thermal oxidation, as shown in Figure S5c. On the other hand, the areal fraction related to Cu^{2+} slightly increased to 3.56% under the HE condition (Figure S6a,c). This result indicates that the bulk-like morphology of sintered layers under the HE condition could effectively prevent oxidation at the top surface. At the 70 nm depth from the surface, the areal fraction related to the Cu^{2+} peaks of the Cu film under the LE condition increased to 28.53% after thermal oxidation in Figure S5d, while that under the HE condition was not significantly changed (Figure S6d). This means that the passivating layer and thick sintered layer could prevent oxidation.

Therefore, it can be concluded that the Cu film sintered under the HE condition exhibited a thin and stable CuO layer based on the XPS results of the top surface after thermal oxidation. The preformed CuO layer can act as a passive layer preventing further surface oxidation, and the low thickness of this layer facilitates the movement of electrons owing to the high tunneling transmission. These results were similar to the oxidation trends observed for bulk Cu substrates. In contrast, Cu film sintered under the LE condition exhibited a thick CuO layer, which hinders the movement of electrons owing to the low tunneling transmission.

For the evaluation of thermal oxidation resistance, Cu tracks sintered by IPL and LPEB under the LE and HE conditions were projected to electrical conductivity measurements under a high temperature (220 °C). As shown in Figure 4d, the resistance of Cu tracks sintered by IPL initially showed good electrical conductivity (∼1.2 Ω) due to its connected structure like HE (Figure S2b,c). However, the electrical resistance of the IPL sample was vulnerable to oxidation in the air at elevated temperatures due to its thin sintered layer, which reduces the path of electrons at a higher rate than the thick sintered layer when it oxidized. Therefore, the electrical resistance of the IPL sample rapidly increased to 4.7−5.3 MΩ after 30 min at 220 °C. The electrical resistance of Cu tracks under the LE condition also significantly increased from 3.0 Ω to 1.8−3.4 MΩ after 30 min at 220 °C. This can be attributed to the formation of a thick oxide layer owing to the individual formation of CuO nanoislands on each CuNP. This thick oxide layer hinders the electrical conduction because of the exponential decay of the tunneling transmission coefficient. In contrast, the resistance of Cu tracks under the HE condition gradually increased from 1.2 to 30−100 Ω at 220 °C for 3 h. The electrical conductivity variations of LPEB-sintered Cu tracks under the HE condition showed promising results; thus, it can be adopted as an electrode for high-temperature applications without using any chemical additives or other materials. To the best of our knowledge, this is the first report in this field of thermal oxidation suppression using only CuNPs in comparison to the use of other noble substances such as silver, CNT, and graphene.

Table 1 shows the comparison of thermal annealing, IPL, laser sintering, and LPEB in terms of pressure condition, processing time, substrate damage, large-scale sintering possibility, patternability, the thickness of the sintered layer, and oxidation resistance.[51,52] The substrates irradiated by IPL or the laser are able to keep their quality without damage, while the thermal annealing and the LPEB can damage the substrate due to exposure to high temperatures and high kinetic energy of electrons, respectively. The laser sintering can draw complex patterns with high resolution without masks. IPL and LPEB can also produce simple patterns with masks. However, the thermal annealing process cannot be adopted for patterning of the printed electrode because there is no straightness of the heat sources unlike other techniques, which means that the patterning is not possible even with a mask. However, for large-scale sintering, thermal annealing, IPL, and LPEB can sinter at once, while the laser sintering takes a long time for the large area due to its narrow sintering

https://doi.org/10.1021/acsomega.1c02475
ACS Omega 2021, 6, 19134−19143

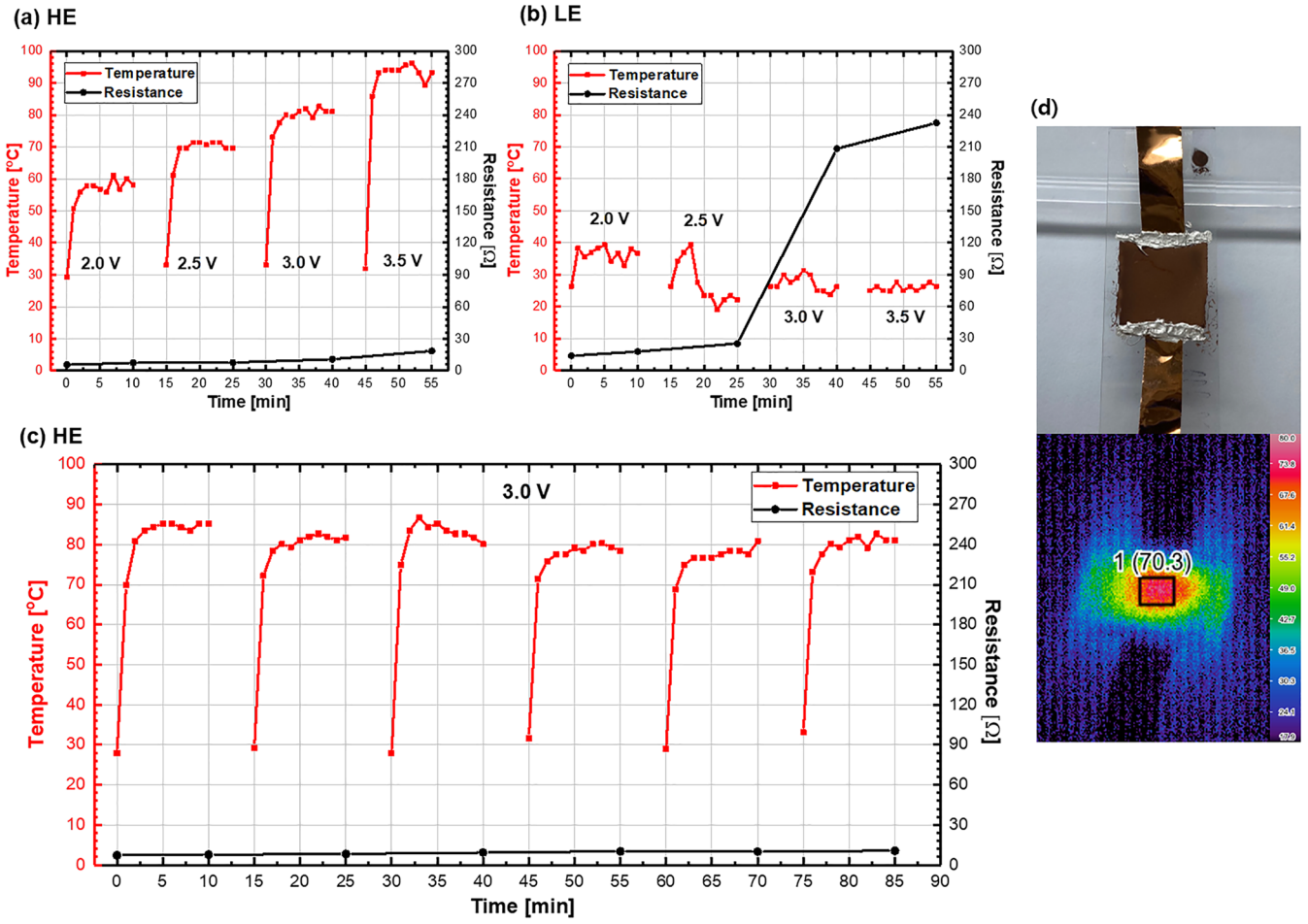

Figure 5. Variation of temperature and electrical resistance on copper films sintered by LPEB under the (a) HE and (b) LE conditions using different applied voltages from 2.0 to 3.5 V. (c) Repeated Joule heating measurements on the copper film sintered by LPEB under the HE condition with consecutive 3.0 V application. (d) Images of the Joule heater during the operation captured by optical and infrared cameras.

area. Photon-based post-treatments (IPL and laser) can be processed under ambient condition, resulting in a short processing time. However, they have poor oxidation resistance due to the thin sintered layer. LPEB takes a relatively long time to operate once due to the requirement of a vacuum environment in Ar gas (0.05 Pa). However, they have good oxidation resistance.

2.4. Joule Heating Performance of Cu Films under HE and LE Conditions. The most important factor for using printed electrodes as a Joule heater is the conserving electrical resistance of the electrodes regardless of the heat. The Joule heater system composed of the conductive Cu tracks sintered using LPEB irradiation was constructed to demonstrate the application of the oxidation resistance of Cu films. The electrical resistance and temperature changes of Cu films irradiated under the HE and LE conditions were determined with different applied voltages of 2.0, 2.5, 3.0, and 3.5 V (Figure 5a,b). After increasing the temperature by Joule heating, the Cu film sintered under the HE condition maintained stable temperature under different voltages because of the bulk-like electrical property of the deep-sintered Cu layer, as shown in Figure 5a. Depending on the increase in the applied voltage, the temperature of the Cu film sintered under the HE condition increased to ~100 °C at 3.5 V and the electrical resistance was maintained in the range of a few ohms. In contrast, the Cu film sintered under the LE condition lost its function as a Joule heater at voltage >2.5 V because of the weak thermal oxidation resistance of the thin sintered Cu layer, as shown in Figure 5b. Additionally, the electrical resistance increased up to the 100 Ω range. To ensure the repeatability of Cu film sintering under the HE condition at a high temperature (80 °C), a cyclic test was performed on the Cu film with consecutive 3.0 V (Figure 5c) application. The Cu film sintered under the HE condition showed consistent performance of Joule heating and also maintained its electrical resistance. Figure 5d shows the nearly uniform and stable temperature profiles after the sixth cycle. In conclusion, the deep-sintered Cu film under the HE condition was able to maintain its electrothermal performance and electrical property at high temperatures because of the strong thermal oxidation resistance like bulk Cu without any additional material.

3. CONCLUSIONS

In this study, the manufacturing of printed Cu film as conductive tracks was demonstrated. The sintering process of CuNPs and Cu formate using LPEB under the HE condition enhanced thermal oxidation resistance without adding any other substances such as Ag, CNT, and GnP. The conductive tracks maintained their electrical conductivity at high temperatures similar to bulk Cu by deep-sintering that originated from the unique interaction and transmission between the electron beam and Cu film. Web-like connections, thick

https://doi.org/10.1021/acsomega.1c02475
ACS Omega 2021, 6, 19134−19143

Table 2. Parameters of Large Pulsed Electron Beam Irradiation on Copper Nanoparticles for the Sintering Processes

sample ID	acceleration voltage [kV]	number of pulses	processing time [min]	solenoid voltage [kV]	anode voltage [kV]	argon pressure [Pa]	pulse duration [μs]
low energy	8	60	40	1	5	0.05	~2
high energy	11	15	24				

sintered layer, and small surface area were formed, and they effectively prevented the oxidation by forming the deep-sintered Cu layer. For the performance evaluation, a Joule heater was fabricated using the LPEB-sintered Cu film under the HE condition, and it showed great potential in terms of Joule heater application with only CuNPs being able to maintain its electrothermal characteristics despite repeated uses. This novel technique of sintering process using LPEB demonstrates the great potential as a breakthrough in solving the challenging problem of printed electronics using metallic NPs, oxidation.

4. EXPERIMENTAL SETUP

4.1. Preparation of F-Cu Inks. CuNPs with an average diameter of 100 nm (TEKNA, Quebec, Canada) were prepared for the LPEB sintering process. Poly(*N*-vinyl-pyrrolidone) (MW: 40 000 g/mol), diethylene glycol (DEG), and formic acid (HCOOH) were purchased from Sigma-Aldrich. F-Cu inks were formed by sonicating 1 g of CuNPs with 0.1 g of PVP dissolved in 1.5 mL of HCOOH and 3 mL of DEG. HCOOH removes the Cu oxide layer of CuNPs. PVP was used not only to act as an adhesive between NPs but also to facilitate the reduction of the oxide shells of CuNPs.[53] Using F-Cu inks, Cu films were fabricated using the doctor-blade method onto the glass slides with a square patterned mask with 20 mm length. Thereafter, the Cu films were dried on a hot plate at 120 °C for 30 min to evaporate the solvents. The thickness of the as-prepared Cu films was approximately 50 μm, as shown in Figure S7.

4.2. Sintering Process of Cu Films. The LPEB irradiation can induce a rapid thermal gradient with a few microseconds pulse duration on the Cu film surface. During repeated irradiation, the surface of Cu film melted and resolidified.[32,42,47,54] Electrons were accelerated through electric and magnetic fields induced by the solenoid between the cathode and anode. Abundant anions and electrons were generated when the electron cloud induced numerous ion−electron collisions near the anode. LPEB irradiation proceeded in a vacuum chamber filled with Ar gas (0.05 Pa) to form plasma under different irradiation conditions. The schematic of LPEB is illustrated in Figure 1. The accelerated electrons, which have very high kinetic energy, irradiated from the LPEB induced unique interactions with substrates, such as scattering, backscattering, and transmission.[42] The electrons passing through atoms of substrates can deeply penetrate the substrates when they are far from the nucleus, which is referred to as transmission. In contrast, the accelerating path of electrons can be refracted when they pass through the sphere of influence around nucleus, which is called elastic scattering. The energy reflection of accelerated electrons can be observed when the accelerating path is significantly refracted, changing to the opposite direction, which is called backscattering. Additionally, inelastic scattering occurs when the incident electrons and electrons in the nucleus perfectly collide.[55,56] Most of the electron energy is absorbed by substrates at a specific depth because the absorptivity of accelerated electrons can be determined as a function of penetration depth, indicating that most electrons having high kinetic energy convert their energy to heat energy due to collision at the specific depth. Moreover, the conduction of heat starts from the depth absorbing the maximum energy, then the energy propagated to the upper and lower regions from depth absorbing the maximum energy.[42]

The total energy transferred by LPEB irradiation can be affected by numerous parameters, such as pulse duration, irradiation distance, cathode voltage, and number of pulses. In this study, the pulse duration and dwell time of the LPEB irradiation were fixed at 2 μs and 10 s, respectively. The diameter of the beam was 60 mm for the sintering process. The irradiating energy was mainly controlled by two processing parameters: (1) cathode voltage and (2) the number of irradiations. First, an increase in the cathode voltage can generate a high energy transfer during a single pulse, leading to an increase in the penetration depth of the accelerated electrons. Second, the number of pulses can affect the total energy transferred from the LPEB irradiation, maintaining the power of a single pulse. The results of optimization steps are summarized in Figure S8. Two representative conditions that can successfully sinter the Cu film were specified: (1) a high cathode voltage (11 kV) and a low number of pulses (15 pulses), which can be referred to as the high energy (HE) condition and (2) a low cathode voltage (8 kV) and a large number of pulses (60 pulses), which can be referred to as low energy (LE) condition. The detailed conditions for the LPEB irradiation are summarized in Table 2. For comparison with LPEB sintering, intensive pulsed light (IPL) irradiation was adopted as a sintering process of Cu film. IPL irradiation with a power of 4 kW and a pulse duration of 6 ms was performed on the identical Cu film under ambient conditions.

4.3. Characterization. The Cu film morphology was observed using scanning electron microscopy (SEM, Nanonova 230, FEI). The elemental analysis of the Cu film before and after thermal oxidation was performed using an energy-dispersive X-ray system equipped with SEM. Crystalline phase analysis was performed using X-ray diffraction (XRD, D8 ADVANCE, Bruker AXS) with Cu Kα radiation source. The potential was 40 kV, the current was 40 mA, and the variation over 2θ ranged from 20 to 80° with a 0.02° step size. Chemical composition analysis according to depth was performed using depth profiling X-ray photoelectron spectroscopy (XPS, K-Alpha, Thermo Fisher) with Al Kα radiation source. The energy emission was analyzed with a pass energy of 50 eV and an energy step size of 0.1 eV. Depth profiling was performed by ion etching at every 100 s. For the thermal oxidation tests, three different types of Cu films (IPL-sintered, LPEB-sintered with LE and HE conditions) were prepared. And the bulk Cu block was prepared following the polishing process as a reference. Each sintered Cu film was heated on a hot plate at 220 °C in an ambient atmosphere. The resistance of the Cu films was measured using the two-point probe method. For the Joule heater demonstration, the circuit was prepared by applying different voltages of 2.0, 2.5, 3.0, and 3.5 V using a

https://doi.org/10.1021/acsomega.1c02475
ACS Omega 2021, 6, 19134−19143

DC-regulated source applied to the Cu films sintered under the HE and LE conditions. Moreover, for repeatability test, the voltage of 3.0 V was consecutively applied to the Cu film under the HE condition. The temperature change and the thermographic data of the surface of Cu films were perceived through an infrared camera (NEC Thermo Tracer, NEC Avio Infrared Technologies Co. Ltd., model No. H2640) with an accuracy of ±2% of reading at a working distance of approximately 30 cm.

■ ASSOCIATED CONTENT

Supporting Information

The Supporting Information is available free of charge at https://pubs.acs.org/doi/10.1021/acsomega.1c02475.

X-ray photoelectron spectroscopy spectra before and after LPEB irradiation; surface and cross-sectional scanning electron micrographs of the as-prepared Cu film fabricated using the doctor-blade method; scanning electron micrographs of the IPL-sintered Cu film: cross-sectional and top views; comparison of microstructures between conductive copper tracks sintered by LPEB irradiation under the LE and HE conditions; variation of resistance on bulk Cu substrates in terms of thermal oxidation time; and deconvolution of XPS spectra on LPEB-sintered Cu films using LE and HE conditions (PDF)

■ AUTHOR INFORMATION

Corresponding Authors

Jisoo Kim − *Department of Advanced Science and Technology Convergence, Kyungpook National University (KNU), Sangju-si, Gyeongsangbuk-do 37224, Republic of Korea; Department of Precision Mechanical Engineering, Kyungpook National University (KNU), Sangju-si, Gyeongsangbuk-do 37224, Republic of Korea;* orcid.org/0000-0001-9540-2800; Phone: +82-54-530-1279; Email: js.kim@knu.ac.kr; Fax: +82-54-530-1278

Changyong Yim − *Department of Advanced Science and Technology Convergence, Kyungpook National University (KNU), Sangju-si, Gyeongsangbuk-do 37224, Republic of Korea; School of Nano & Materials Science and Engineering, Kyungpook National University (KNU), Sangju-si, Gyeongsangbuk-do 37224, Republic of Korea;* orcid.org/0000-0001-5987-9580; Phone: +82-54-530-1335; Email: cy.yim@knu.ac.kr; Fax: +82-54-530-1339

Hyung Wook Park − *School of Mechanical and Nuclear Engineering, Ulsan National Institute of Science and Technology (UNIST), Ulsan 44919, Republic of Korea;* orcid.org/0000-0002-7751-1402; Phone: +82-52-217-2319; Email: hwpark@unist.ac.kr; Fax: +82-52-217-2409

Author

Yunjae Hwang − *School of Mechanical and Nuclear Engineering, Ulsan National Institute of Science and Technology (UNIST), Ulsan 44919, Republic of Korea*

Complete contact information is available at: https://pubs.acs.org/10.1021/acsomega.1c02475

Notes

The authors declare no competing financial interest.

■ ACKNOWLEDGMENTS

This work was supported by the National Research Foundation (NRF) of Korea grant funded by the Korea government (MSIT) (nos. 2020R1F1A1071775 and 2020R1G1A1099886) and the Ministry of Education (no. 2021R1I1A3045191).

■ REFERENCES

(1) Khan, Y.; Thielens, A.; Muin, S.; Ting, J.; Baumbauer, C.; Arias, A. C. A New Frontier of Printed Electronics: Flexible Hybrid Electronics. *Adv. Mater.* **2020**, *32*, No. 1905279.

(2) Arias, A. C.; MacKenzie, J. D.; McCulloch, I.; Rivnay, J.; Salleo, A. Materials and Applications for Large Area Electronics: Solution-Based Approaches. *Chem. Rev.* **2010**, *110*, 3−24.

(3) Huang, Q.; Zhu, Y. Printing Conductive Nanomaterials for Flexible and Stretchable Electronics: A Review of Materials, Processes, and Applications. *Adv. Mater. Technol.* **2019**, *4*, No. 1800546.

(4) Kamyshny, A.; Magdassi, S. Conductive Nanomaterials for Printed Electronics. *Small* **2014**, *10*, 3515−3535.

(5) Papanastasiou, D. T.; Schultheiss, A.; Muñoz-Rojas, D.; Celle, C.; Carella, A.; Simonato, J.-P.; Bellet, D. Transparent Heaters: A Review. *Adv. Funct. Mater.* **2020**, *30*, No. 1910225.

(6) Wang, Y.; Chen, L.; Cheng, H.; Wang, B.; Feng, X.; Mao, Z.; Sui, X. Mechanically flexible, waterproof, breathable cellulose/polypyrrole/polyurethane composite aerogels as wearable heaters for personal thermal management. *Chem. Eng. J.* **2020**, *402*, No. 126222.

(7) Zhang, R.; Lin, W.; Moon, K.-s.; Wong, C. P. Fast Preparation of Printable Highly Conductive Polymer Nanocomposites by Thermal Decomposition of Silver Carboxylate and Sintering of Silver Nanoparticles. *ACS Appl. Mater. Interfaces* **2010**, *2*, 2637−2645.

(8) Veeramuthu, L.; Chen, B.-Y.; Tsai, C.-Y.; Liang, F.-C.; Venkatesan, M.; Jiang, D.-H.; Chen, C.-W.; Cai, X.; Kuo, C.-C. Novel stretchable thermochromic transparent heaters designed for smart window defroster applications by spray coating silver nanowire. *RSC Adv.* **2019**, *9*, 35786−35796.

(9) He, P.; Cao, J.; Ding, H.; Liu, C.; Neilson, J.; Li, Z.; Kinloch, I. A.; Derby, B. Screen-Printing of a Highly Conductive Graphene Ink for Flexible Printed Electronics. *ACS Appl. Mater. Interfaces* **2019**, *11*, 32225−32234.

(10) Liang, F.-C.; Chang, Y.-W.; Kuo, C.-C.; Cho, C.-J.; Jiang, D.-H.; Jhuang, F.-C.; Rwei, S.-P.; Borsali, R. A mechanically robust silver nanowire−polydimethylsiloxane electrode based on facile transfer printing techniques for wearable displays. *Nanoscale* **2019**, *11*, 1520−1530.

(11) Ahmed, A.; Jalil, M. A.; Hossain, M. M.; Moniruzzaman, M.; Adak, B.; Islam, M. T.; Parvez, M. S.; Mukhopadhyay, S. A PEDOT:PSS and graphene-clad smart textile-based wearable electronic Joule heater with high thermal stability. *J. Mater. Chem. C* **2020**, *8*, 16204−16215.

(12) Kim, H.; Jang, J. I.; Kim, H. H.; Lee, G.-W.; Lim, J. A.; Han, J. T.; Cho, K. Sheet Size-Induced Evaporation Behaviors of Inkjet-Printed Graphene Oxide for Printed Electronics. *ACS Appl. Mater. Interfaces* **2016**, *8*, 3193−3199.

(13) Jiang, D.-H.; Tsai, P.-C.; Kuo, C.-C.; Jhuang, F.-C.; Guo, H.-C.; Chen, S.-P.; Liao, Y.-C.; Satoh, T.; Tung, S.-H. Facile Preparation of Cu/Ag Core/Shell Electrospun Nanofibers as Highly Stable and Flexible Transparent Conductive Electrodes for Optoelectronic Devices. *ACS Appl. Mater. Interfaces* **2019**, *11*, 10118−10127.

(14) Cardenas, J. A.; Catenacci, M. J.; Andrews, J. B.; Williams, N. X.; Wiley, B. J.; Franklin, A. D. In-Place Printing of Carbon Nanotube Transistors at Low Temperature. *ACS Appl. Nano Mater.* **2018**, *1*, 1863−1869.

(15) Deng, D.; Jin, Y.; Cheng, Y.; Qi, T.; Xiao, F. Copper Nanoparticles: Aqueous Phase Synthesis and Conductive Films Fabrication at Low Sintering Temperature. *ACS Appl. Mater. Interfaces* **2013**, *5*, 3839−3846.

(16) Vaithilingam, J.; Simonelli, M.; Saleh, E.; Senin, N.; Wildman, R. D.; Hague, R. J. M.; Leach, R. K.; Tuck, C. J. Combined Inkjet

Printing and Infrared Sintering of Silver Nanoparticles using a Swathe-by-Swathe and Layer-by-Layer Approach for 3-Dimensional Structures. *ACS Appl. Mater. Interfaces* **2017**, *9*, 6560−6570.
(17) Lim, H. S.; Kim, S. J.; Jang, H. W.; Lim, J. A. Intense pulsed light for split-second structural development of nanomaterials. *J. Mater. Chem. C* **2017**, *5*, 7142−7160.
(18) Määttänen, A.; Ihalainen, P.; Pulkkinen, P.; Wang, S.; Tenhu, H.; Peltonen, J. Inkjet-Printed Gold Electrodes on Paper: Characterization and Functionalization. *ACS Appl. Mater. Interfaces* **2012**, *4*, 955−964.
(19) Yim, C.; Sandwell, A.; Park, S. S. Hybrid Copper−Silver Conductive Tracks for Enhanced Oxidation Resistance under Flash Light Sintering. *ACS Appl. Mater. Interfaces* **2016**, *8*, 22369−22373.
(20) Yim, C.; Kockerbeck, Z. A.; Jo, S. B.; Park, S. S. Hybrid Copper−Silver−Graphene Nanoplatelet Conductive Inks on PDMS for Oxidation Resistance Under Intensive Pulsed Light. *ACS Appl. Mater. Interfaces* **2017**, *9*, 37160−37165.
(21) Perelaer, J.; Smith, P. J.; Mager, D.; Soltman, D.; Volkman, S. K.; Subramanian, V.; Korvink, J. G.; Schubert, U. S. Printed electronics: the challenges involved in printing devices, interconnects, and contacts based on inorganic materials. *J. Mater. Chem.* **2010**, *20*, 8446−8453.
(22) Jung, J.; Cho, H.; Choi, S. H.; Kim, D.; Kwon, J.; Shin, J.; Hong, S.; Kim, H.; Yoon, Y.; Lee, J.; Lee, D.; Suh, Y. D.; Ko, S. H. Moiré-Free Imperceptible and Flexible Random Metal Grid Electrodes with Large Figure-of-Merit by Photonic Sintering Control of Copper Nanoparticles. *ACS Appl. Mater. Interfaces* **2019**, *11*, 15773−15780.
(23) Kwon, J.; Cho, H.; Suh, Y. D.; Lee, J.; Lee, H.; Jung, J.; Kim, D.; Lee, D.; Hong, S.; Ko, S. H. Flexible and Transparent Cu Electronics by Low-Temperature Acid-Assisted Laser Processing of Cu Nanoparticles. *Adv. Mater. Technol.* **2017**, *2*, No. 1600222.
(24) Kang, B.; Ko, S.; Kim, J.; Yang, M. Microelectrode fabrication by laser direct curing of tiny nanoparticle self-generated from organometallic ink. *Opt. Express* **2011**, *19*, 2573−2579.
(25) Ryu, C.-H.; Joo, S.-J.; Kim, H.-S. Intense pulsed light sintering of Cu nano particles/micro particles-ink assisted with heating and vacuum holding of substrate for warpage free printed electronic circuit. *Thin Solid Films* **2019**, *675*, 23−33.
(26) Park, S.-H.; Kim, H.-S. Flash light sintering of nickel nanoparticles for printed electronics. *Thin Solid Films* **2014**, *550*, 575−581.
(27) Kang, H.; Sowade, E.; Baumann, R. R. Direct Intense Pulsed Light Sintering of Inkjet-Printed Copper Oxide Layers within Six Milliseconds. *ACS Appl. Mater. Interfaces* **2014**, *6*, 1682−1687.
(28) Jeong, S.; Woo, K.; Kim, D.; Lim, S.; Kim, J. S.; Shin, H.; Xia, Y.; Moon, J. Controlling the Thickness of the Surface Oxide Layer on Cu Nanoparticles for the Fabrication of Conductive Structures by Ink-Jet Printing. *Adv. Funct. Mater.* **2008**, *18*, 679−686.
(29) Yabuki, A.; Tanaka, S. Oxidation behavior of copper nanoparticles at low temperature. *Mater. Res. Bull.* **2011**, *46*, 2323−2327.
(30) Dai, X.; Xu, W.; Zhang, T.; Shi, H.; Wang, T. Room temperature sintering of Cu-Ag core-shell nanoparticles conductive inks for printed electronics. *Chem. Eng. J.* **2019**, *364*, 310−319.
(31) Hwang, H.-J.; Joo, S.-J.; Kim, H.-S. Copper Nanoparticle/Multiwalled Carbon Nanotube Composite Films with High Electrical Conductivity and Fatigue Resistance Fabricated via Flash Light Sintering. *ACS Appl. Mater. Interfaces* **2015**, *7*, 25413−25423.
(32) Kim, J.; Lee, W. J.; Park, H. W. The state of the art in the electron beam manufacturing processes. *Int. J. Precis. Eng. Manuf.* **2016**, *17*, 1575−1585.
(33) Kim, J.; Park, S. S.; Park, H. W. Corrosion inhibition and surface hardening of KP1 and KP4 mold steels using pulsed electron beam treatment. *Corros. Sci.* **2014**, *89*, 179−188.
(34) Kim, J.; Nam, Y. S.; Song, M. H.; Park, H. W. Large Pulsed Electron Beam Welded Percolation Networks of Silver Nanowires for Transparent and Flexible Electrodes. *ACS Appl. Mater. Interfaces* **2016**, *8*, 20938−20945.
(35) Murr, L. E.; Gaytan, S. M.; Ramirez, D. A.; Martinez, E.; Hernandez, J.; Amato, K. N.; Shindo, P. W.; Medina, F. R.; Wicker, R. B. Metal Fabrication by Additive Manufacturing Using Laser and Electron Beam Melting Technologies. *J. Mater. Sci. Technol.* **2012**, *28*, 1−14.
(36) Körner, C. Additive manufacturing of metallic components by selective electron beam melting — a review. *Int. Mater. Rev.* **2016**, *61*, 361−377.
(37) López-Delgado, A.; Cano, E.; Bastidas, J. M.; López, F. A. A comparative study on copper corrosion originated by formic and acetic acid vapours. *J. Mater. Sci.* **2001**, *36*, 5203−5211.
(38) Cano, E.; Torres, C. L.; Bastidas, J. M. An XPS study of copper corrosion originated by formic acid vapour at 40% and 80% relative humidity. *Mater. Corros.* **2001**, *52*, 667−676.
(39) Ratke, L. *Growth and Coarsening Ostwald Ripening in Material Processing*, 1st ed.; Voorhees, P. W., Ed.; Springer: Berlin, Heidelberg, 2002.
(40) Hansen, T. W.; DeLaRiva, A. T.; Challa, S. R.; Datye, A. K. Sintering of Catalytic Nanoparticles: Particle Migration or Ostwald Ripening? *Acc. Chem. Res.* **2013**, *46*, 1720−1730.
(41) Meyers, R. A. *Encyclopedia of Physical Science and Technology*, 3rd ed.; Academic Press: San Diego, 2002.
(42) Kim, J.; Lee, W. J.; Park, H. W. Temperature predictive model of the large pulsed electron beam (LPEB) irradiation on engineering alloys. *Appl. Therm. Eng.* **2018**, *128*, 151−158.
(43) Zheng, C.; Cao, J.; Zhang, Y.; Zhao, H. Insight into the Oxidation Mechanism of a Cu-Based Oxygen Carrier (Cu → Cu2O → CuO) in Chemical Looping Combustion. *Energy Fuels* **2020**, *34*, 8718−8725.
(44) Rana, F.; Tiwari, S.; Buchanan, D. A. Self-consistent modeling of accumulation layers and tunneling currents through very thin oxides. *Appl. Phys. Lett.* **1996**, *69*, 1104−1106.
(45) French, A. P. *An Introduction to Quantum Physics*, 1st ed.; Taylor, E. F., Ed.; Norton: New York, 1978.
(46) Quanli, J.; Haijun, Z.; Suping, L.; Xiaolin, J. Effect of particle size on oxidation of silicon carbide powders. *Ceram. Int.* **2007**, *33*, 309−313.
(47) Kim, J.; Park, H. W. Influence of a large pulsed electron beam (LPEB) on the corrosion resistance of Ti−6Al−7Nb alloys. *Corros. Sci.* **2015**, *90*, 153−160.
(48) Zhang, Z.; Yang, S.; Lv, P.; Li, Y.; Wang, X.; Hou, X.; Guan, Q. The microstructures and corrosion properties of polycrystalline copper induced by high-current pulsed electron beam. *Appl. Surf. Sci.* **2014**, *294*, 9−14.
(49) Kocijan, A.; Merl, D. K.; Jenko, M. The corrosion behaviour of austenitic and duplex stainless steels in artificial saliva with the addition of fluoride. *Corros. Sci.* **2011**, *53*, 776−783.
(50) Stellwag, B. The mechanism of oxide film formation on austenitic stainless steels in high temperature water. *Corros. Sci.* **1998**, *40*, 337−370.
(51) Park, B. K.; Kim, D.; Jeong, S.; Moon, J.; Kim, J. S. Direct writing of copper conductive patterns by ink-jet printing. *Thin Solid Films* **2007**, *515*, 7706−7711.
(52) Niittynen, J.; Sowade, E.; Kang, H.; Baumann, R. R.; Mäntysalo, M. Comparison of laser and intense pulsed light sintering (IPL) for inkjet-printed copper nanoparticle layers. *Sci. Rep.* **2015**, *5*, No. 8832.
(53) Hwang, H.-J.; Chung, W.-H.; Kim, H.-S. In situmonitoring of flash-light sintering of copper nanoparticle ink for printed electronics. *Nanotechnology* **2012**, *23*, No. 485205.
(54) Uno, Y.; Okada, A.; Uemura, K.; Raharjo, P.; Sano, S.; Yu, Z.; Mishima, S. A new polishing method of metal mold with large-area electron beam irradiation. *J. Mater. Process. Technol.* **2007**, *187−188*, 77−80.
(55) Cosslett, V. E.; Thomas, R. N. Multiple scattering of 5-30 keV electrons in evaporated metal films II: Range-energy relations. *Br. J. Appl. Phys.* **1964**, *15*, 1283−1300.
(56) Cosslett, V. E.; Thomas, R. N. Multiple scattering of 5 - 30 keV electrons in evaporated metal films III: Backscattering and absorption. *Br. J. Appl. Phys.* **1965**, *16*, 779−796.

https://doi.org/10.1021/acsomega.1c02475
ACS Omega 2021, 6, 19134−19143